Nonconserved Residues Ala287 and Ser290 of the *Cryptosporidium hominis* Thymidylate Synthase Domain Facilitate Its Rapid Rate of Catalysis[†,‡]

Lanxuan T. Doan, W. Edward Martucci, Melissa A. Vargo, Chloé E. Atreya, and Karen S. Anderson*

Department of Pharmacology, Yale University School of Medicine, 333 Cedar Street, New Haven, Connecticut 06520

Received March 15, 2007; Revised Manuscript Received May 16, 2007

ABSTRACT: *Cryptosporidium hominis* TS-DHFR exhibits an unusually high rate of catalysis at the TS domain, at least 10-fold greater than those of other TS enzymes. Using site-directed mutagenesis, we have mutated residues Ala287 and Ser290 in the folate-binding helix to phenylalanine and glycine, respectively, the corresponding residues in human and most other TS enzymes. Our results show that the mutant A287F, the mutant S290G, and the double mutant all have reduced affinities for methylene tetrahydrofolate and reduced rates of reaction at the TS domain. Interestingly, the S290G mutant enzyme had the lowest TS activity, with a catalytic efficiency ∼200-fold lower than that of the wild type (WT). The rate of conformational change of the S290G mutant is ∼80 times slower than that of WT, resulting in a change in the rate-limiting step from hydride transfer to covalent ternary complex formation. We have determined the crystal structure of ligand-bound S290G mutant enzyme, which shows that the primary effect of the mutation is an increase in the distance between the TS ligands. The kinetic and crystal structure data presented here provide the first evidence explaining the unusually fast TS rate in *C. hominis*.

Thymidylate synthase (TS) and dihydrofolate reductase (DHFR) are targets for chemotherapy of infectious diseases and cancer since they are essential for the proliferation of cells. Thymidylate synthase catalyzes the reaction of deoxyuridine monophosphate (dUMP)[1] and methylene tetrahydrofolate (CH_2H_4folate) to yield deoxythymidine monophosphate (dTMP) and dihydrofolate (H_2folate) (Scheme 1) (*1*). DHFR catalyzes the reduction of H_2folate, in the presence of nicotinamide adenine dinucleotide phosphate (NADPH), to generate tetrahydrofolate (H_4folate) (*2*). Tetrahydrofolate is required for several biological processes, including the syntheses of dTMP, purines, and amino acids. TS and DHFR are highly conserved and generally are expressed as individual monofunctional enzymes (*1*, *3*). However, in protozoans (and some plants), DHFR and TS exist as a bifunctional enzyme in which they are expressed on a single polypeptide (*4*, *5*). Studies show that the bifunctional TS-DHFR enzymes may exhibit unique functionalities as a consequence of the dual catalytic activities. At a structural level, the interplay between these activities is mediated by domain−domain communication and substrate channeling between the TS and DHFR domains (*6*, *7*). We have previously studied the reactions of TS-DHFR from *Cryptosporidium hominis* (*Ch*), and it was discovered that *Ch*TS-DHFR shows a very high rate of activity at the TS domain, ∼10−40 fold faster than those of other TS enzymes (*8*).

Thymidylate synthase is a highly conserved enzyme in both sequence and structure. While the *Ch*TS domain displays overall conservation, it contains two nonconserved residues, Ala287 and Ser290, in the folate-binding domain (Figure 1A), whereas in most species, these residues are phenylalanine and glycine. While some TS species contain a change at one of the positions, only the unusually fast *C. hominis* TS has both an alanine and a serine. It is noteworthy that the *Bacillus subtilis* TS-A, which has an alanine and a threonine, also has a high catalytic TS rate (*9*). The phenylalanine at position 287 has been implicated in folate binding (*10*, *11*). In the crystal structure of *Ch*TS-DHFR, Ser290 forms a hydrogen bond with the glutamate tail of the folate cofactor, CB3717, an interaction not observed in other TS enzymes (Figure 1B) (*12*). Additionally, both residues are part of the folate-binding helix, which contains residues that are essential for catalysis (*13*).

In this study, we used site-directed mutagenesis to investigate the effects of residues Ala287 and Ser290 on the activity of the bifunctional *Ch*TS-DHFR enzyme. In addition, we have determined the crystal structure of the S290G mutant enzyme to offer a physical explanation of the importance of this residue. Both residues discussed here lie within the folate-binding domain, a key site for the design of species-specific inhibitors (*14*). A full understanding of how these species-unique TS residues influence this enzyme's catalytic cycle is essential, since there are currently no antiparasitic drugs available for *C. hominis*, the opportunistic pathogen that causes cryptosporidiosis (*15*).

[†] This work was supported in part by NIH Grant AI 44630 and NIH Parasitology Grant A10740414.

[‡] The coordinates for the structure reported in this work have been deposited in the Protein Data Bank under the file name 2OIP.

* To whom correspondence should be addressed. Telephone: (203) 785-4526. Fax: (203) 785-7670. E-mail: karen.anderson@yale.edu.

[1] Abbreviations: TS-DHFR, thymidylate synthase-dihydrofolate reductase (this is a functional designation as dihydrofolate is produced at TS and used at DHFR; elsewhere, the bifunctional enzyme is termed DHFR-TS because DHFR resides at the N-terminal portion of the bifunctional protein); dUMP, deoxyuridine monophosphate; dTMP, deoxythymidine monophosphate; CH_2H_4folate, methylene tetrahydrofolate; H_2folate, dihydrofolate; H_4folate, tetrahydrofolate; NADPH, nicotinamide adenine dinucleotide phosphate; CB3717, 10-propargyl L-5,8-dideazafolate; HPLC, high-performance liquid chromatography.

10.1021/bi700531r CCC: $37.00
Published on Web 06/20/2007

Scheme 1

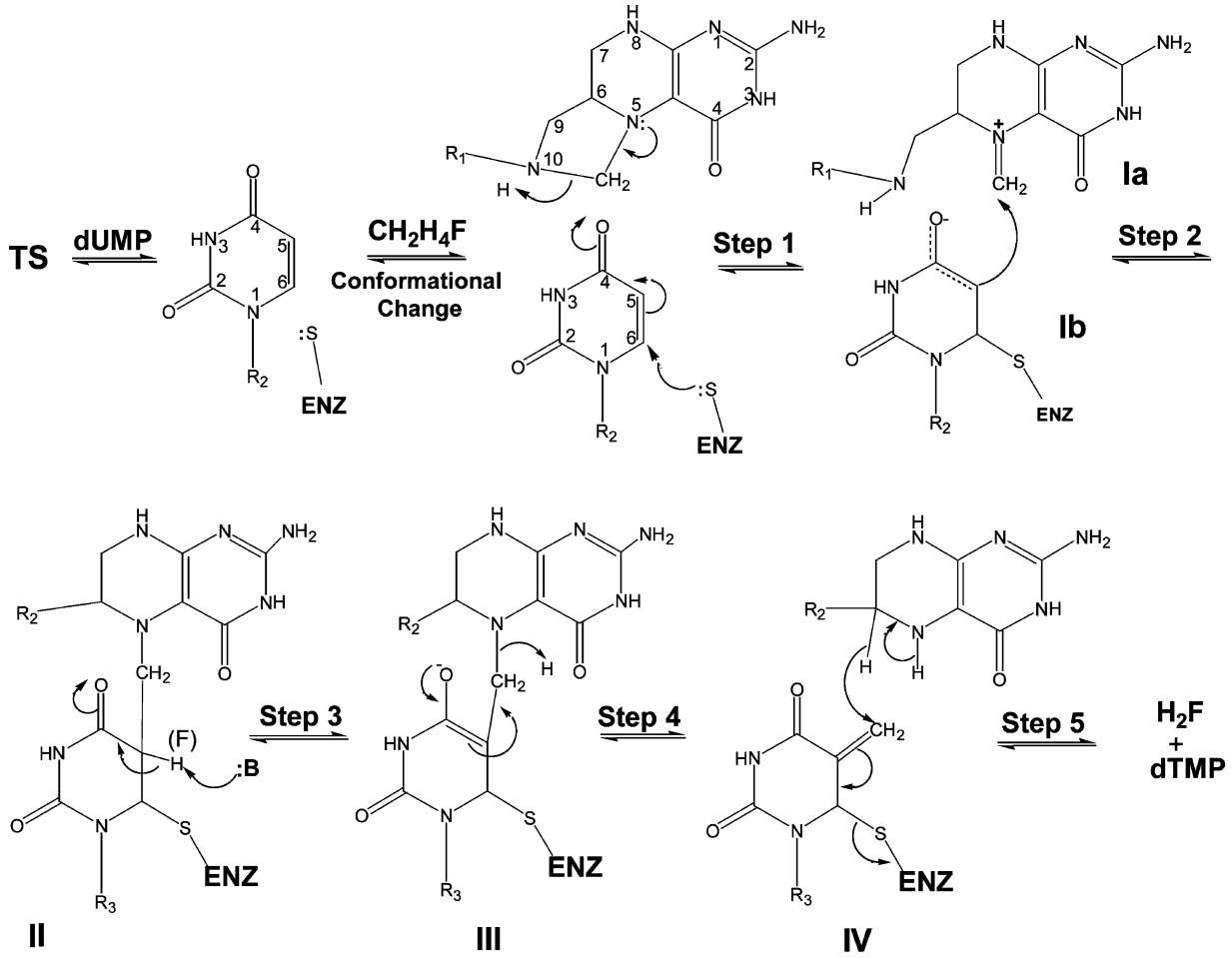

MATERIALS AND METHODS

Chemicals and Reagents. All buffers and other reagents employed were of the highest commercial purity. Millipore ultrapure water was used for all solutions. 7,8-Dihydrofolate (H_2folate) was chemically prepared by the reduction of folate with sodium hydrosulfite. (6*R*,*S*)-5,6,7,8-Tetrahydrofolate was obtained from Schirks Laboratories. Radiolabeled H_2-folate was synthesized by sodium hydrosulfite reduction of tritium-labeled [3′,5′,7,9-^{3}H]folic acid obtained from Moravek Biochemicals (Brea, CA). Radiolabeled and unlabeled CH_2H_4-folate were prepared by enzymatic conversion of radiolabeled and unlabeled H_2folate, respectively, which forms (6*R*,*S*)-5,6,7,8-tetrahydrofolate and subsequent condensation with formaldehyde (*16*). Both H_2folate and CH_2H_4folate were purified using DE-52 anion exchange resin (Whatman Co.) and elution using a linear gradient of triethylammonium bicarbonate (*17*). [2-^{14}C]dUMP (52 mCi/mmol) was obtained from Moravek Biochemicals. The concentrations of all substrates were determined spectrophotometrically, according to previously published extinction coefficients (*18*, *19*). Experiments were carried out at 25 °C in 50 mM Tris buffer (pH 7.8) containing 1 mM EDTA, 25 mM $MgCl_2$, and 10 mM DTT. Buffer solutions were purged with argon prior to use.

*Protein Expression and Purification. Ch*TS-DHFR was purified according to a previously published protocol (*8*). Site-directed mutations were created using a QuikChange mutagenesis kit (Stratagene). Plasmids containing the desired mutations, as confirmed by nucleic acid sequencing, were used to transform competent *Escherichia coli* BL21-DE3 cells, and proteins were purified in a manner similar to that of the wild type. The concentration of TS-DHFR protein was estimated by a Bio-Rad assay with BSA as a standard.

Enzyme Activity. The DHFR activity was determined by monitoring the decrease in absorbance at 340 nm ($\Delta\epsilon = -12800\ M^{-1}\ cm^{-1}$), following the enzymatic conversion of NADPH and H_2folate to $NADP^+$ and H_4folate, as previously described. The TS activity was determined by following the increase in absorbance at 340 nm ($\Delta\epsilon = 6400\ M^{-1}\ cm^{-1}$) for the conversion of substrates dUMP and CH_2H_4folate to products dTMP and H_2folate at 25 °C as previously described (*20*).

*Spectrophotometric TS Assay. Ch*TS-DHFR (10, 30, or 120 nM) was preincubated with dUMP (100 μM) prior to being mixed with CH_2H_4folate (0.5−350 μM), and the absorbance was monitored at 340 nm using a Hewlett-Packard 8452A spectrophotometer. Initial rates were determined in duplicate using the software provided by the instrument, and these rates were converted to units of specific activity using the reported extinction coefficient for the reaction ($\Delta\epsilon_{rxn} = 6400\ M^{-1}\ cm^{-1}$).

Rapid Chemical Quench. Rapid chemical quench experiments were performed using a Kintek RFQ-3 rapid chemical quench apparatus (Kintek Instruments, Austin, TX). The reactions were initiated by mixing an enzyme solution (15 μL) with the radiolabeled substrate (15 μL, approximately

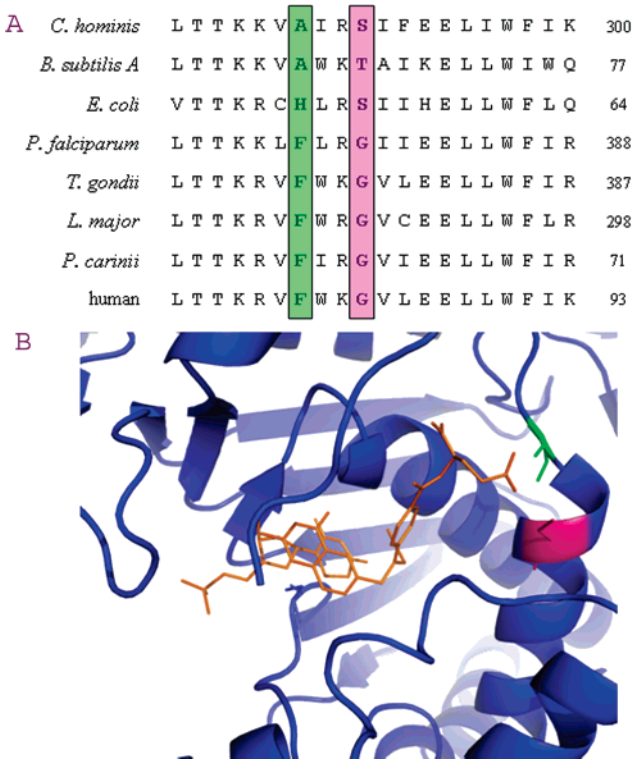

FIGURE 1: Wild-type *Ch*TS active site. (A) Alignment of the partial TS sequence consisting of the folate-binding helix and flexible loop, with positions 287 and 290 highlighted. (B) *Ch*TS (PDB entry 1qzf) ligands are colored orange; dUMP is in the background, and CB3717 is in the foreground. Ala287 is colored green and Ser290 violet.

35 000 dpm for [^{3}H]folates and 20 000 dpm for [2-^{14}C]-dUMP). In all cases, the concentrations of enzyme and substrates cited in the text are those after mixing and during the reaction. For TS pre-steady-state burst experiments, *Ch*TS-DHFR (25 μM) was preincubated with 500 μM dUMP and then reacted with 75 μM CH_2H_4folate. For TS single-enzyme turnover experiments, the *Ch*TS-DHFR enzyme (100 μM) was preincubated with a saturating concentration of dUMP (500 μM) and then mixed with a limiting concentration of radiolabeled CH_2H_4folate (10 μM). To assess the DHFR reaction under single-turnover conditions, enzyme (100 μM) was preincubated with a saturating concentration of NADPH (500 μM) and then mixed with a limiting concentration of radiolabeled H_2folate (10 μM).

Reactions utilizing radiolabeled folates were terminated by quenching with base (0.78 N KOH) as described previously. For reactions in which radiolabeled dUMP and dTMP were utilized, 0.4 M HCl was used for quenching (*8*). To confirm complete quenching of the enzymatic reactions, controls in which substrate was added to a premixed solution of enzyme and quench solution were included with each experiment.

HPLC Analysis. A portion (~70 μL) of each quenched reaction solution was quantified by radio-HPLC. Separation was performed using a BDS-Hypersil C18 reverse phase column (250 mm × 4.6 mm, Keystone Scientific, Bellefonte, PA), as previously described (*8*). When the intermediate peak was separated from the H_2folate peak, the pH of the elution buffer was adjusted to pH 8.5, allowing for separation of the folate intermediate, H_2folate, and CH_2H_4folate peaks, and an elution profile is shown in Figure S1 of the Supporting Information. The elution profile for the separation of dUMP and dTMP is shown in Figure S2 of the Supporting Information.

Data Analysis. Rapid chemical quench data were analyzed using the curve fitting program GraphPad Prism. Stopped-flow measurements provided estimates for the association and dissociation rate constants (k_{on} and k_{off}, respectively) and for reaction rate constants. Comparison of rapid chemical quench and stopped-flow reaction time courses allowed for the assignment of observed stopped-flow rates to chemical steps or conformational changes.

Stopped-Flow Fluorescence Measurements. Stopped-flow measurements were performed using a Kintek SF-2001 apparatus (Kintek Instruments) as detailed previously (*8*). Fluorescence changes were monitored following excitation at 287 nm and emission at 340 nm. To assess the binding of enzyme with CB3717, the monochromator was set at 287 nm on the input and the FRET was monitored with an interference filter at 380 nm to determine k_{on} and a 340 nm cutoff filter to measure k_{off}. An average of three to five runs was fit to a single-exponential, double-exponential, or burst equation to obtain rate constants.

The TS protein conformational change upon substrate binding was followed by setting the monochromator to 287 nm on the input and monitoring the change in intrinsic enzyme fluorescence with an output filter at 340 nm. The *Ch*TS-DHFR enzyme (4 μM) was preincubated with 500 μM dUMP and buffer and then mixed with CH_2H_4folate (2−350 μM) or CB3717 (1−20 μM). For DHFR, NADPH coenzyme fluorescence resonance energy transfer (FRET) experiments were carried out with 290 nm excitation and an output filter at 450 nm. In DHFR burst experiments, 7.5 μM enzyme was preincubated with 50 μM H_2folate and buffer and then mixed with 500 μM NADPH. In single-enzyme turnover experiments, 50 μM enzyme was preincubated with 500 μM NADPH and buffer and then mixed with 10 μM H_2folate.

SDS−PAGE of the Ternary Covalent Intermediate. SDS−PAGE gels were used to detect the enzyme−dUMP−CH_2H_4-folate ternary covalent complex (**II** and **III** in Scheme 1), as previously described with minor modifications (*13*, *21*). Instead of using 1% SDS and 10% β-mercaptoethanol to quench the reactions, we used 200 mM β-mercaptoethanol in 0.4 M HCl. Collected samples were placed on ice for 20 min and spun down to pellet the precipitated protein. The protein pellets were washed with water, resuspended in SDS loading buffer, and analyzed according to the published procedure (*13*, *21*).

Kinetic Simulation. The KinTekSim kinetic simulation program (version 3.0.3) was used to model the catalytic mechanisms of reactions for the TS domain of wild-type and S290G *Ch*TS-DHFR (*8*, *19*). Minimal mechanistic schemes were written, and parameters were adjusted to fit to the experimental kinetic data.

Crystallization and Data Collection. Pure *Ch*TS-DHFR S290G mutant protein was incubated at a final concentration of 7 mg/mL with 1 mM ligands (dUMP, CB3717, NADPH, and methotrexate) for 45 min on ice. The protein/ligand mix was crystallized using the hanging-drop vapor diffusion technique. The successful well solution consisted of 0.1 mM ammonium sulfate, 0.3 M lithium sulfate, 0.1 M Tris, and 10% polyethylene glycol 6000. Crystals with approximate

Table 1: Values of k_{cat}, K_m, and Efficiency from Steady-State Kinetics[a]

	k_{cat} (s^{-1})[b]	K_m[CH_2H_4folate] (μM)	efficiency (k_{cat}/K_m)
WT	11.7 ± 0.2	2.7 ± 1.2	4.3
A287F	8.2 ± 0.3	10.1 ± 2.2	0.81
S290G	0.8 ± 0.2	48.2 ± 1.8	0.02
double mutant	7.6 ± 0.3	8.7 ± 2.5	0.87

[a] Values are an average from duplicate trials. [b] The turnover number is calculated considering that TS exists as a dimer and is a half-sites reactive enzyme. Thus, the turnover number is the number of moles of product formed per second per mole of active subunit (one-half the moles of total enzyme used).

dimensions of 0.3 mm × 0.1 mm × 0.05 mm grew in 1 week at 18 °C. Crystals were soaked in successive cryoprotectants of mother liquor with 10 and 25% ethylene glycol for 2 min each and were flash-frozen in liquid nitrogen.

Diffraction data were collected at the Brookhaven National Laboratory on beamline X25. Our best crystal diffracted to 2.7 Å. Data were indexed, integrated, and scaled to 2.8 Å using HKL2000 (*22*) and were converted to structure factors with Truncate (*23*). Five percent of the reflections were marked for cross-validation analysis to serve as R_{free}. The structure of the WT *Ch*TS-DHFR enzyme was determined on similar instruments at the same facility and scaled and refined using the same software, allowing us to make comparisons between that structure and the one presented here.

Structure Solution. The structure of the *Ch*TS-DHFR S290G mutant cocrystallized with ligands was determined using the coordinates of wild-type *Ch*TS-DHFR (Protein Data Bank entry 1QZF), with waters and ligands removed, as a starting model. Since the protein crystallized with the same space group and unit cell, we could begin direct refinement. After a rigid-body fit using Refmac5 from the CCP4 suite (*24*), the initial *R*-factor was 40% and, when the domains were allowed to move independently, was lowered to 36%. The negative difference density for the absent Ser290 side chain was evident in the initial difference map in every monomer. Additionally, all of the ligands were visible in the initial $F_o - F_c$ difference maps. The structure was refined using Refmac5; density modification was conducted using Solomon (*23*), and iterative processes of refinement and manual residue and ligand positioning were carried out in the visualization programs O (*25*) and COOT (*26*). After addition of waters in Refmac5, group *B*-factor refinement in CNS (*27*), and geometry optimization, the final R_{fac} was 22.1 and R_{free} was 26.0. All refinement statistics are reported in Table 5. The structure was deposited in Protein Data Bank as entry 2OIP.

RESULTS

Steady-State Analysis of TS and DHFR Activities of Wild-Type and Mutant Enzymes. To characterize the effects of these residues, we created S290G, A287F, and the double mutant (A287F/S290G) and steady-state kinetics were used to provide an initial assessment of the catalytic activities. The k_{cat} values for TS activities for WT, A287F, S290G, and the double mutant are 11.7, 8.2, 0.8, and 7.6 s^{-1}, respectively (Table 1). However, the rate of activity of the DHFR domain appeared not to be affected. Within experimental error, WT and mutant enzymes have DHFR activities of ~3 s^{-1}. The K_m values of WT *Ch*TS, A287F, S290G, and the double mutant for CH_2H_4folate are determined to be 2.7, 10, 48, and 9 μM, respectively (Table 1). The drastic effect of the mutations is best demonstrated in the value of catalytic efficiency (k_{cat}/K_m), where the values for A287F and the double mutant are ~5-fold lower and that of S290G is ~200-fold lower than that of WT (Table 1). Overall, this demonstrates that the affinities of the mutant enzymes for CH_2H_4folate and their activities at the TS domain are significantly altered.

Single-Enzyme Turnover and Pre-Steady-State Burst Experiments for Examining the DHFR Reaction. To confirm that there was no impact of the A287F and S290G mutations on the activity of the DHFR domain, we performed single-enzyme turnover experiments using rapid chemical quench. Fitting the data to a single-exponential equation yielded a rate constant of ~128 s^{-1} for WT and mutant enzymes (data not shown). We also monitored the DHFR activity by stopped-flow techniques. Under pre-steady-state burst conditions, the data were fit to a burst equation to yield a burst rate of ~124 s^{-1} and a steady-state rate of 3.1 s^{-1} (Figure S3A of the Supporting Information). Within statistical errors, the DHFR domains of WT and mutant enzymes all have the same rates of reactions.

Pre-Steady-State Burst for the TS Reaction. As a first step in dissecting the mechanism for the TS reaction, we examined the WT *Ch*TS reaction under pre-steady-state conditions. The rate profile shows a burst rate of approximately 175 s^{-1} and a burst amplitude of 13.0 μM. The burst amplitude indicates the active site concentration, which is one-half of the enzyme concentration that was used. This indicates that *Ch*TS, like the monofunctional TS enzyme, is a half-the-sites reactive enzyme (*28*). Dividing the slope of the linear portion of the plot by the amplitude gives a steady-state rate of 12.4 s^{-1}.

Single-Enzyme Turnover Experiments for Examining the TS Reaction. To more precisely evaluate chemistry, single-enzyme turnover experiments with WT and mutant enzymes were carried out on a rapid chemical quench apparatus. The time courses for the consumption of CH_2H_4folate by WT and mutant enzymes are shown in Figure 2. The rate profiles of WT, A287F, and the double mutant show biphasic behavior; however, the S290G mutant does not. Specifically, Figure 2A demonstrates that the WT rate profile fits better to a double-exponential equation (solid line) than to a single-exponential equation (dotted line). Fitting the data from the reaction of WT *Ch*TS to a double-exponential equation yields a very fast phase with a rate constant k_1 of ~250 s^{-1} and a slower phase with a rate constant k_2 of 27 s^{-1}. The mutants yield reaction rates slower than that of WT (Figure 2B,C and Table 2): the rate of catalysis of the double mutant is ~2-fold slower than that of the wild type, while the S290G mutant is >10-fold slower.

Affinity of WT and Mutant ChTS Domains for Folate Analogues. Another method for determining the affinity of TS for its folate cofactor is utilizing the folate analogue CB3717 (also called propargyl dideazafolate or PDDF). CB3717 is structurally very similar to CH_2H_4folate (Figure 3) (*29*), and conveniently, CB3717 has a fluorescence emission at 380 nm (*8*). As shown previously, CB3717 binds to the bifunctional TS enzymes in the presence or absence

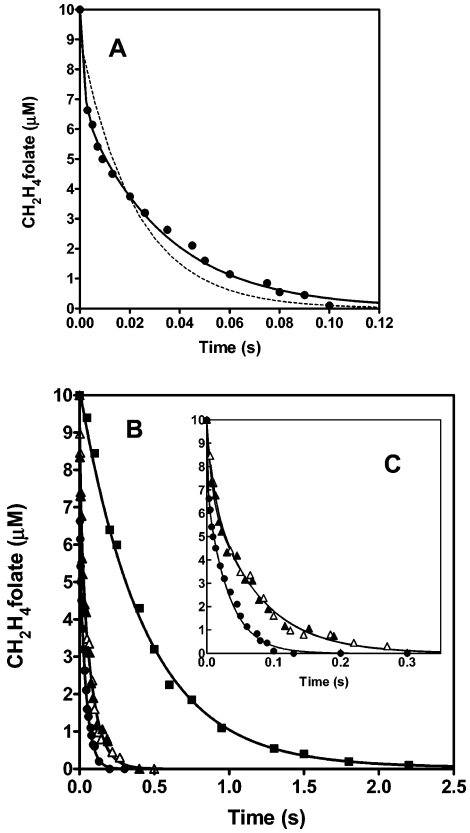

FIGURE 2: Reaction time courses for the consumption of CH_2H_4-folate from single-enzyme turnover of WT and mutant *Ch*TS. (A) WT data fit to single-exponential (- - -) and double-exponential (—) equations. (B and C) Time courses for WT (●), the A287F mutant (△), the double mutant (▲), and the S290G mutant (■).

Table 2: Rate Constants from TS Single-Enzyme Turnover Reactions Fit to Single- and Double-Exponential Equations

	single-exponential fit	double-exponential fit	
	k_1 (s^{-1})[a]	k_1 (s^{-1})[b]	k_2 (s^{-1})[c]
WT	46.0 ± 7.2	~250 ± 30	27.3 ± 0.5[d]
A287F	18.5 ± 2.5	133 ± 9	13.5 ± 0.9[d]
S290G	2.3 ± 0.1[d]	NA	NA
double mutant	18.0 ± 2.3	110 ± 11	13.6 ± 0.7[d]

[a] k_1 corresponds to k_{chem} (catalytic rate) for the single-exponential fit. [b] k_1 corresponds to the rate of conformational change preceding catalysis in the double-exponential fit. [c] k_2 corresponds to k_{chem} (catalytic rate) for the double-exponential fit. [d] Most accurate value for k_{chem} based on the best fit to either single- or double-exponential equations.

of dUMP (*8*), Therefore, the k_{on} rate of CB3717 was obtained by mixing 100 nM *Ch*TS-DHFR with increasing concentrations of CB3717. As shown in Figure 4A, the fluorescence change associated with binding of CB3717 to the enzyme is biphasic, with a fast CB3717 concentration-dependent phase (k_{obs}) and a slow concentration-independent phase of 6 s^{-1}. Plotting k_{obs} versus the concentration of CB3717, where $k_{obs} = k_{on}[CB3717] + k_{off}$, yields a k_{on} of 42 s^{-1} μM^{-1}. The k_{off} was measured independently in a competition experiment in which the TS-DHFR was preincubated with CB3717 and mixed with excess CH_2H_4F; the k_{off} was determined to be 2.0 s^{-1}. Within experimental error, the affinities of WT and mutant enzymes (Table 3, left columns) for CB3717 are the same, with a K_d of approximately 50 nM. These results are consistent with those previously published (*8*). Additionally, our results show that the association of CB3717 with *Ch*TS-DHFR is similar either in the presence or in the absence of dUMP, and the affinity of WT or mutant *Ch*TS for dUMP is similar (data not shown) and corresponds to the previously published K_d value of 35 μM (*8*).

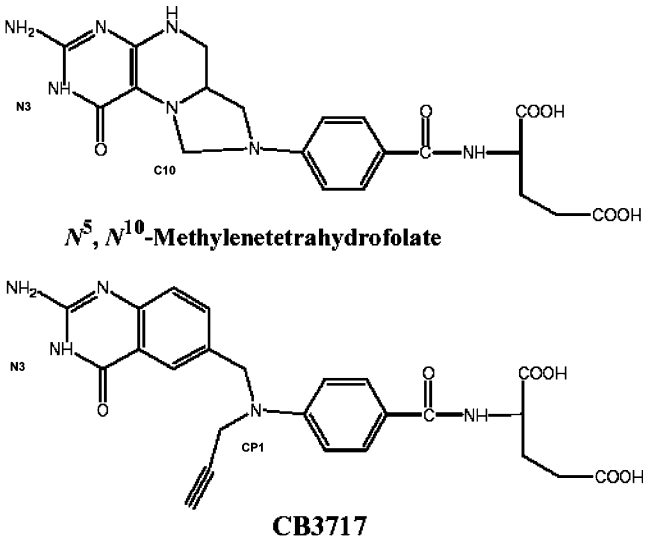

FIGURE 3: Structures of CH_2H_4folate and CB3717.

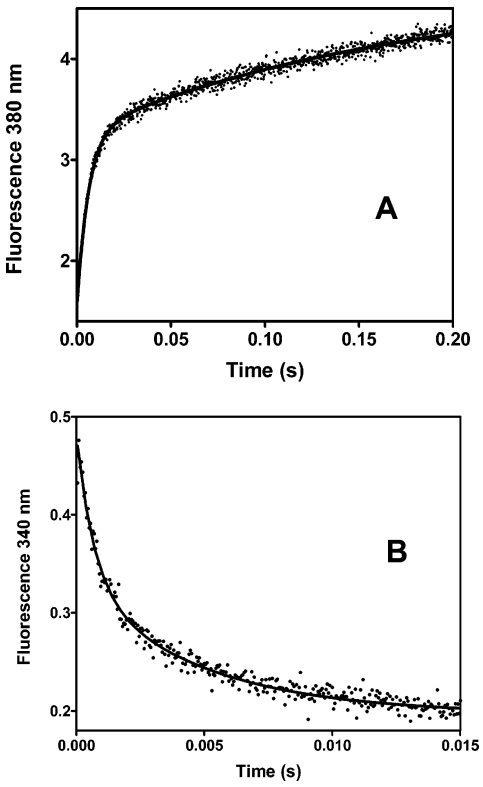

FIGURE 4: Stopped-flow experiments assessing conformational change. (A) Representative stopped-flow trace of fluorescence at 380 nm vs time, observed upon mixing *Ch*TS-DHFR (100 nM) with 5.0 μM CB3717. (B) Representative stopped-flow trace of fluorescence at 340 nm vs time, in which WT *Ch*TS-DHFR (3 μM) was preincubated with 500 μM dUMP followed by mixing with 100 μM CH_2H_4folate.

Conformational Changes Associated with Folate Binding. Numerous studies have demonstrated that monofunctional TS enzymes (from *E. coli*, *Lactobacillus casei*, and humans) undergo conformational changes upon binding of folate cofactors (*3*, *30*−*32*). To evaluate whether residues Ser290 and Ala287 affect the conformation of the TS domain, we

Table 3: Dissociation Constants of Folate Cofactors for WT and Mutant Enzymes[a]

	CB3717			CH_2H_4folate		
	k_{off} (s^{-1})	k_{on} (μM^{-1} s^{-1})	K_d (μM)	k_{off} (s^{-1})	k_{on} (μM^{-1} s^{-1})	K_d (μM)
WT	2.1	42	0.050	100	21.1	4.7
A287F	2.0	45	0.044	77	5.1	15.1
S290G	2.0	41	0.049	7.4	0.19	38.9
double mutant	1.9	44	0.043	81	4.7	17.2

[a] The error associated with the determination of each rate constant is <10% in all cases.

Table 4: Rates of Conformational Changes Upon Ligand Binding from Monitoring the Fluorescence Change at 340 nm[a]

	CB3717 (20 μM)		CH_2H_4folate (100 μM)	
	k_1 (s^{-1})[b]	k_2 (s^{-1})[c]	k_1 (s^{-1})[b]	k_2 (s^{-1})[c]
WT	>500	76	>500	300
A287F	>500	81	~400	128
S290G	>500	79	27.4	3.7
double mutant	>500	72	~400	120

[a] The error associated with the determination of each rate constant is <10% in all cases. [b] Concentration-dependent rate constant associated with binding of folate cofactor. [c] Concentration-independent rate constant following the binding of CB3717 or CH_2H_4folate.

compared the intrinsic fluorescence change of WT and mutant enzymes in the presence of ligands. When CB3717 was mixed with the dUMP−enzyme complex, the fluorescence change at 340 nm was biphasic. WT and mutant enzymes have the same rates of conformational changes with a very fast concentration-dependent phase (corresponding to binding) and a slower concentration-independent phase of 75 s^{-1} (corresponding to conformational change following binding). Plotting this fast concentration-dependent phase yields the same value for k_{on} for CB3717 as seen above (Tables 3 and 4, left columns).

Mixing of CH_2H_4folate with the enzyme−dUMP complex was also biphasic. However, in contrast to CB3717, differences in the rates of fluorescence changes were observed. Both phases of fluorescence changes increase with increasing concentrations of CH_2H_4folate. When the CH_2H_4folate concentration was 100 μM, the first rate, k_1, is very fast (>500 s^{-1}) for WT (Table 4, right columns). This is likely due to the conformational change associated with binding of CH_2H_4folate. A representative stopped-flow trace for WT is shown in Figure 4B. The plot of the WT rates from the first phase versus the concentration of CH_2H_4folate yields a k_{on} of 21 μM^{-1} s^{-1} and a k_{off} of 100 s^{-1}, and thus, $K_d = 4.7$ μM (Table 3, right column). Compared to WT, the mutant enzymes have lower affinities for CH_2H_4folate, with K_d values of 15, 39, and 17 μM for the A287F mutant, the S290G mutant, and the double mutant, respectively (Table 3, right columns). The rate of the second phase of fluorescence change for WT is slower and reaches a maximum value of 300 s^{-1} (Table 4, right column). This rate correlates with the value of k_1 for the rate of consumption of CH_2H_4folate from the single-enzyme turnover reaction of WT *Ch*TS (Table 2). This is also true for the mutant enzymes.

For WT, the rates of conformational changes are very fast (Table 4, right columns), with a k_1 of >500 s^{-1} and a k_2 of ~300 s^{-1}. The rates of conformational changes for the mutants are slower than that of WT (Table 4, right columns).

Table 5: Data Collection and Refinement Statistics for the Structure of the *Ch*TS-DHFR S290G Mutant Enzyme Complexed with dUMP, CB3717, NADPH, and Methotrexate[a]

resolution limit (Å)	2.80
space group	*C*2
unit cell parameters	215.0 Å, 116.2 Å, 216.6 Å, 90°, 94.27°, 90°
no. of reflections used	130114
completeness (%)	99.2 (98.7)
redundancy	3.3
I/σ	9.3 (2.9)
R_{merge} (%)	11.7 (53.8)
no. of monomers in the asymmetric unit	5
refinement statistics	
R_{factor} (%)	22.1
R_{free} (%)	26.0
total no. of atoms	21926
no. of water molecules	399
rmsd for bonds (Å)	0.009
rmsd for angles (deg)	1.4
Wilson *B* factor (Å^2)	65
average *B* factor, non-H atoms (Å^2)	66
coordinate error, Luzzati (Å)	0.38
Ramachandran plot	
residues in most favored regions (%)	88.3
residues in additionally allowed regions (%)	10.9
residues in generously allowed regions (%)	0.7
residues in disallowed regions (%)	0.1

[a] Values in parentheses are for the highest-resolution shell.

Specifically, the A287F and double mutants undergo conformational changes at a rate ~2.5-fold slower than that of WT. S290G shows an even greater effect, more than 80-fold slower than the rate of conformational change of the WT enzyme.

Detecting Intermediates from the TS Reactions by HPLC Analyses. Our earlier studies on *Toxoplasma gondii* and *C. hominis* TS-DHFR have reported the observation of an unknown intermediate peak from the TS reaction by HPLC analysis (*8*, *19*). This peak is observed when radiolabeled CH_2H_4folate is used and the reaction is quenched with base. Under single-enzyme turnover conditions for the WT TS reaction, the maximum level of accumulation of this folate-intermediate is ~38% at 22 ms (Figure 5A). In the case of the S290G mutant, the maximum level of accumulation of this intermediate is ~8% at 250 ms (Figure 5B).

Determining the Rate of dTMP Formation. Since our results demonstrate that the rate of CH_2H_4folate consumption is biphasic for WT but not for the S290G mutant, we examined the rate of formation of dTMP. Under pre-steady-state conditions, the rate of formation of dTMP does not show a burst for WT or S290G (Figure S2B of the Supporting Information). This indicates that the limiting step in the TS reaction is not release of product.

We also determined the rate of formation of dTMP under single-turnover conditions. For WT, the rate of formation of dTMP (65 s^{-1}) (Figure S2C of the Supporting Information) is different from the rate of consumption of CH_2H_4folate (27 s^{-1}) (Figure 2A). A similar situation occurs in the S290G mutant. The S290G mutant has a rate constant of 4.4 s^{-1} for the formation of dTMP (Figure S2D of the Supporting Information), and 2.3 s^{-1} (Table 2) for the disappearance of CH_2H_4folate. The discrepancy may be due to the differences in how the analyses were performed. When the rate of

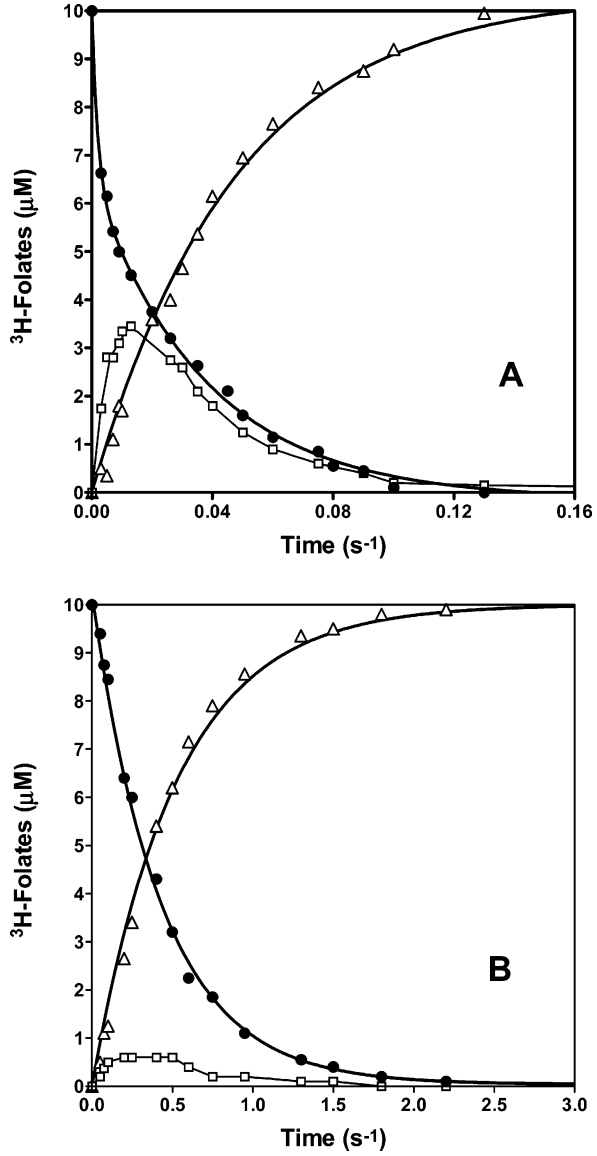

FIGURE 5: Single-enzyme turnover reactions for WT *Ch*TS and the S290G mutant. Rapid chemical quench data from reactions of WT *Ch*TS (A) and S290G (B). Time course for [^{3}H]CH_2H_4folate (●), folate intermediate (□), and H_2folate (△).

consumption of CH_2H_4folate was analyzed, base was utilized to quench the reaction; however, acid was utilized to quench the reaction when the rate of formation of dTMP was assessed. When base quench is used, all reactants, intermediates, and products are observed. When acid quench is used, only *dissociated* dUMP and dTMP are observed and any other covalent intermediates are precipitated with the enzyme. Therefore, formation of dTMP appears to be faster because the intermediates are removed before HPLC analysis. It has been reported that by using acid to precipitate the enzyme, a covalent intermediate of the enzyme−dUMP−CH_2H_4folate complex (**II** and **III**, Scheme 1) can be detected (*33*) and isolated by SDS−PAGE (*13*). For these reasons, we set out to try to isolate the covalent ternary complex with SDS−PAGE gels.

Discerning the Covalent Ternary Intermediate. Studies have detected the covalent ternary intermediate complex by denaturing and isolating the enzyme with SDS gels and counting for radioactivity associated with it. The protein gel band was isolated, dissolved, and counted in scintillation cocktail. The graph of the amount of radioactivity associated with WT enzyme with respect to time is shown in Figure 6A. When [^{3}H]CH_2H_4folate was utilized, similar results were obtained (Figure 6B). A maximum radioactivity of approximately 600−800 cpm was observed at 20 ms and then leveled off at ∼90 ms. The S290G mutant had very little radioactivity associated with it. Under the same conditions that were used for WT, the reaction of the S290G mutant showed radioactivity of ∼200 cpm at 250 ms (Figure 6D,E; note the difference in time scales from WT graphs). These results indicate that for the reaction of WT *Ch*TS, the formation of the enzyme−dUMP−CH_2H_4folate covalent ternary complex is faster, and the complex accumulates to a greater extent than from reaction of the S290G mutant.

The radioactivity associated with the *Ch*TS-DHFR enzyme was analyzed from the reaction of [^{3}H]CH_2H_4folate and FdUMP, a dUMP analogue consisting of a fluorine in place of the proton at the 5-position of the pyrimidine ring (Scheme 1). Due to this substitution, FdUMP is an inhibitor of the TS reaction since there is no longer a hydrogen on C5 to be deprotonated. This, in turn, stops the catalytic reaction at the formation of covalent ternary intermediate **II** (see Scheme 1) (*4*). The plot of radioactivity associated with the WT enzyme from the reaction of FdUMP and [^{3}H]CH_2H_4folate versus time is shown in Figure 6C. The formation of the covalent ternary intermediate is rapid and is saturated very early in the reaction of WT *Ch*TS. In the reaction of S290G, formation of the enzyme−FdUMP−[^{3}H]CH_2H_4folate complex is much slower (Figure 6F). Its formation begins at 100 ms, and since the enzyme−FdUMP−[^{3}H]CH_2H_4folate complex is not converted to product, it slowly continues to form until it is saturated at a much later time (approximately 1−2 s). These results demonstrate slow covalent ternary complex formation as an effect of the S290G mutation.

Kinetic Simulations Suggest a Shift in the Rate-Limiting Step. The KINSIM kinetic program was used to model our rapid chemical quench data obtained from evaluation of the TS domain of WT and S290G *Ch*TS-DHFR (*8*, *19*, *34*). The simulations focused on the minimal catalytic mechanisms for the TS domain from these two enzymes. For WT *Ch*TS, our kinetic simulation suggests that the reaction occurs very rapidly and hydride transfer is the slow step. In the case of the S290G mutant, the overall reaction is much slower than that of WT *Ch*TS. The simulated reaction mechanism suggests that formation of the covalent ternary intermediate may be the slow step. Comparison of the reaction time courses from single-enzyme turnover reactions of WT and S290G and our kinetics modeling is shown in Chart 1. Note the difference in the time scale for WT versus S290G simulated reaction profiles.

X-ray Crystal Structure Solution of the S290G Mutant. To elucidate the structural impact of these nonconserved residues on the enzyme and offer a structural explanation for the kinetic results, the X-ray crystal structure of the *Ch*TS-DHFR S290G mutant enzyme was determined. The construct used for crystal growth was the same as that used for the kinetic studies, the full bifunctional TS-DHFR protein. The ligands at TS were the natural substrate dUMP and the inhibitor CB3717. Instability of CH_2H_4folate precluded its use in crystallization; however, CB3717 has been shown biochemi-

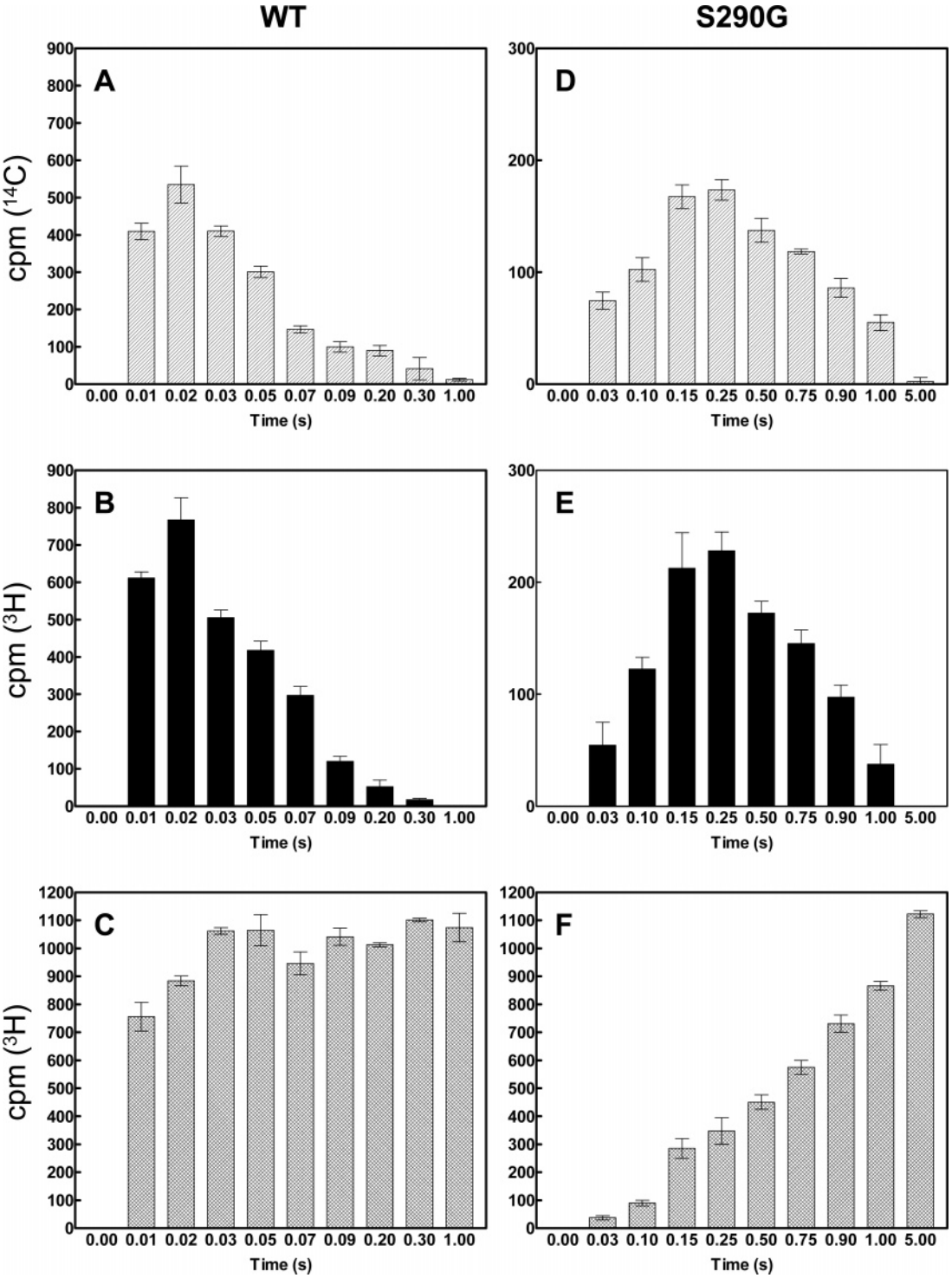

FIGURE 6: Detection of the covalent ternary intermediate by SDS−PAGE. Panels A−C show the radioactivity associated with WT *Ch*TS, and panels D−F show the radioactivity associated with S290G. Panels A and D show reactions in which enzyme was preincubated with [2-^{14}C]dUMP (10 μM) and mixed with excess CH_2H_4folate (500 μM). Note the difference in the time scale. Panels B and E show reactions in which enzyme was preincubated with excess dUMP (500 μM) and mixed with [^{3}H]CH_2H_4folate (10 μM). Panels C and F show reactions utilizing excess FdUMP and limiting [^{3}H]CH_2H_4folate. The amounts of radioactivity for each time point are the average of duplicate determinations with error bars representing the standard deviation.

cally to halt the TS reaction at the covalent intermediate (*35*) and also serves as an accurate model for structural analysis of the TS mechanism (*36*). The crystal asymmetric unit and space group were the same as those of wild-type *Ch*TS-DHFR (*12*), making for an efficient starting model. The initial electron density maps showed that the enzyme crystallizes as the biological dimer, with 5 monomers (2.5 dimers) in the asymmetric unit, and the second half of the final dimer lying across the unit cell axis. There was good electron density for all monomers. All except ~4 residues per monomer had density for their backbone atoms, and all except an additional 3 per monomer had side chain density. These residues were all in the flexible linker region that spans the DHFR domains of a dimer. The residues without any

Chart 1: Minimal Reaction Mechanism and Rate Constants Used To Simulate the WT and S290G *Ch*TS Domain

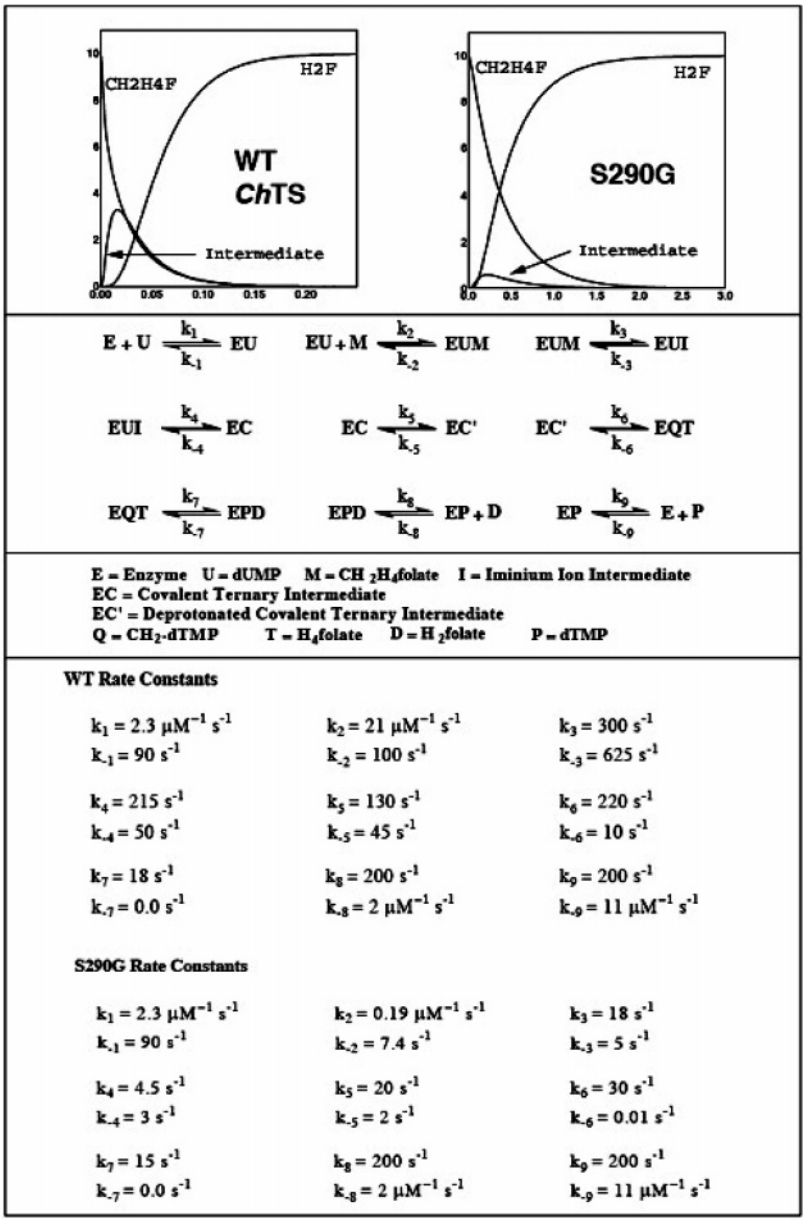

density were deleted, and the residues with no side chain density were built as alanines.

In the initial maps, there was clear negative difference density at -3σ at residue 290 in every monomer, ensuring us that the mutation from serine to glycine was complete in our protein crystals. Additionally, there was electron density for all ligands. The density for all ligands was complete and clearly defined in monomers A, B, and C, except for one carbon−carbon bond in the glutamate tail of CB3717. However, both carboxylates of the tail had strong density and were able to be placed. A representative $F_o - F_c$ composite omit map in Figure 7A demonstrates the complete ligand density, and our ability to confidently fit TS ligands.

Comparison of the S290G Structure with the Wild Type. Comparison of the S290G and wild-type structures showed no changes in the overall enzyme structure and minimal changes in the enzyme active site. There were, however, significant changes in the position of the bound ligands. The overall binding orientations of the substrate dUMP and inhibitor CB3717 are similar in the mutant enzyme, and there is an expected change in conformation of the glutamate tail of CB3717, which hydrogen bonds to Ser290 in the wild-type enzyme (Figure 1). Without the interaction from the nonconserved serine, the glutamate tail shifts up in the active site ~0.5 Å. The effect on the inhibitor is that most atoms in the compound are shifted 0.5−0.8 Å from their position in the wild-type enzyme, pulling the whole compound away from its position in the active site, as seen in Figure 7B. Interestingly, there are also long-range effects of this single mutation on ligand binding, as the position of dUMP is significantly altered. Both the pyrimidine and sugar rings are shifted down and away from their original positions, moving dUMP away from CB3717. The overall effect seems to be greatest on the atoms involved in catalysis [C5 of dUMP and CP1 of CB3717, equivalent to the donated carbon, C10, in CH_2H_4F (Figure 3)]. The distance between the two atoms in wild-type *Ch*TS-DHFR is 3.96 Å, whereas in the S290G enzyme, they move apart by >1.2 Å to a distance of 5.20 Å (Figure 7B).

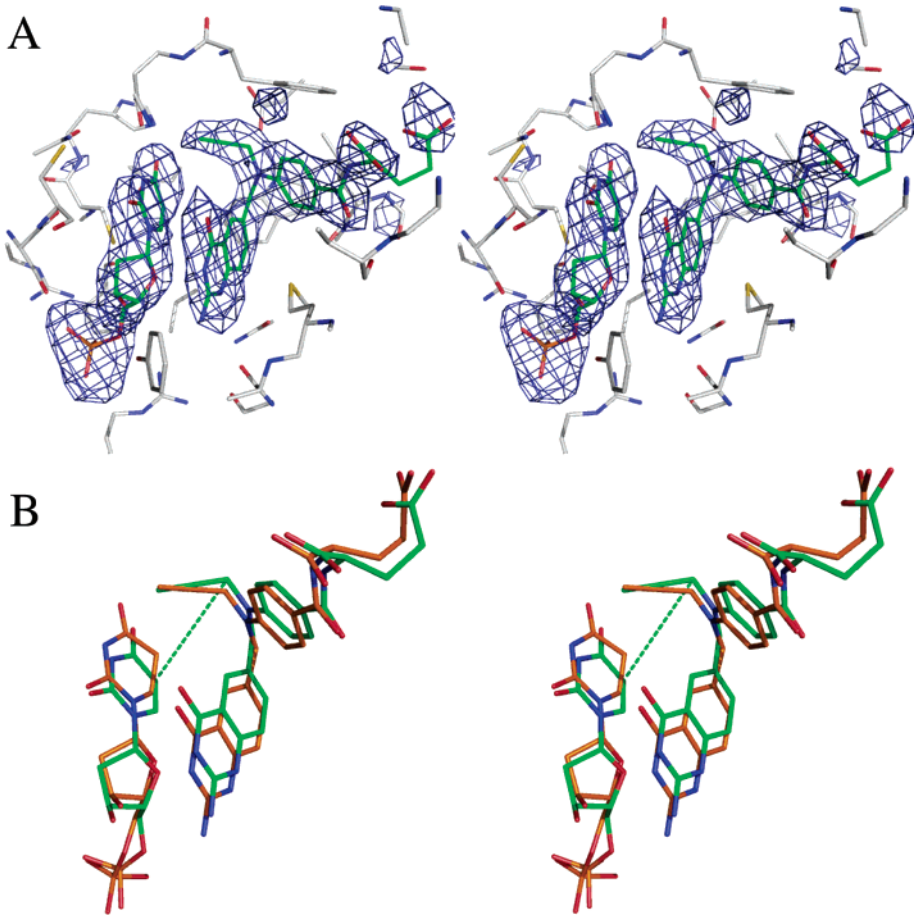

FIGURE 7: TS ligands in the S290G crystal structure. (A) Stereoview omit difference density map (contoured at 2.5σ) of the monomer B active site showing that density is clearly defined for both dUMP and CB3717, including nearly all of the flexible glutamate tail, allowing precise positioning of the ligands. (B) Stereoview comparison of the TS overlay showing the significant movements of the ligands: wild type (orange) and S290G (green). The dashed line highlights the distance increase of 1.2 Å between atoms involved in the catalytic methyl transfer.

DISCUSSION

The bifunctional TS-DHFR enzyme from *C. hominis* exhibits several unique characteristics, one of which is its high rate of activity at the TS domain (*8*). Even though thymidylate synthase is highly conserved, there are subtle differences among species, particularly in the folate-binding region. We have chosen to mutate two nonconserved residues in the folate-binding site, Ala287 and Ser290, to investigate their role in *Ch*TS catalysis. Ala287 and Ser290 were mutated to phenylalanine and glycine, respectively, since these are the corresponding residues in human and most other TS enzymes (*9*, *37*). Our results demonstrate that the A287F and S290G mutations affect the catalytic activity of *Ch*TS and its affinity for CH_2H_4folate. Replacement of the alanine with a phenylalanine at position 287 decreased the affinity of *Ch*TS for CH_2H_4folate by 3-fold. The affinity for CH_2H_4-folate was even lower, a reduction of 8-fold, when Ser290 was mutated to a glycine. However, when both of these mutations occur, as in the case of the double mutant, there appears to be a compensatory effect in which the enzymatic affinity for CH_2H_4folate is reduced only 4-fold. Interestingly, CB3717 binds much more tightly than CH_2H_4folate to the *Ch*TS active site, yet unlike that of CH_2H_4folate, the affinity for CB3717 is unaffected by these mutations. Although CB3717 and CH_2H_4folate are structurally similar, CH_2H_4-folate has a carbon bridge between the N5 and N10 positions, while CB3717 has a propargyl at the N10 position. The difference in the binding of CB3717 and CH_2H_4folate is that binding of CH_2H_4folate requires opening of the imidazolidine ring. Our data show that the rates of conformational change upon binding of CH_2H_4folate are sensitive to mutations of Ala287 and Ser290, while rates of conformational change upon binding of CB3717 are not, suggesting that Ala287 and Ser290 contribute to the ring-opening step in the TS reaction.

From our results, it is apparent that the A287F and S290G mutations decreased the activity of *Ch*TS. Substitution of a glycine for a serine at position 290 showed the most pronounced reduction in TS activity. This mutation also appears to have altered the reaction mechanism of *Ch*TS. The wild-type *Ch*TS reaction is very rapid, and the rate profile for CH_2H_4folate consumption is biphasic. At early time points, the rate of disappearance of CH_2H_4folate (k_1) is approximately 250 s^{-1}. As the catalytic reaction progresses, the rate of disappearance of CH_2H_4folate (k_2) is reduced to approximately 27 s^{-1}. Furthermore, an intermediate is detected from this reaction, and its rate of formation is very rapid. The intermediate accumulates to a relatively high concentration (~35%) and can be detected by SDS gel analyses, which suggest that it is the enzyme−dUMP−CH_2H_4folate ternary covalent complex (**II** and **III** in Scheme 1) (*13*). Consistent with previous kinetic studies on other

TS species (*38*), our kinetic simulations indicate that, in the reaction mechanism of WT *Ch*TS, hydride transfer is the rate-limiting step.

We propose that upon binding of dUMP and CH_2H_4folate, WT *Ch*TS quickly catalyzes the formation of the iminium ion intermediate, **Ia**, and the activated dUMP intermediate, **Ib**. Formation of a bond between these two intermediates yields the covalent ternary intermediate **II**, which is deprotonated to give intermediate **III**. Breakdown of intermediate **III** yields H_4folate and intermediate **IV**. This is followed by rate-limiting hydride transfer from H_4folate to CH_2-dTMP intermediate **IV** to yield dTMP and H_2folate.

However, the reaction of the S290G mutant is different from that of WT *Ch*TS. Its rate of reaction under single-enzyme turnover conditions is slow ($\sim$2.3 s^{-1}) and is not biphasic. Fitting the data to our simulated kinetic mechanism suggests that both the ring-opening step and formation of the covalent ternary intermediate are slow, with the covalent intermediate formation being rate-limiting. Importantly, our SDS gel experiments demonstrate that the formation of the covalent intermediate in the S290G reaction mechanism is very slow, $\sim$3 s^{-1}, confirming this step is rate-limiting.

Determining the X-ray crystal structure of the *Ch*TS-DHFR S290G mutant enzyme has allowed us to examine the structural impact of the single-residue active site mutation and postulate a physical description explaining the kinetic alterations. At this resolution, we caution the use of the X-ray crystal structure alone in interpreting the effect of this mutation. However, the movements we observe provide a logical structural explanation for the detailed kinetic analysis described for the mutant enzyme.

Instead of an effect on the overall enzyme structure, the major consequence of this mutation is a long-range effect on substrate orientation. The loss of interaction of the enzyme with the CB3717 glutamate tail leads to its movement up and away from its original position. This movement pulls it sufficiently far from dUMP to abolish the only hydrogen bond between the two ligands, causing dUMP to slide down and away from its original position. The large decrease in the rate of catalysis in the S290G enzyme seems ultimately to be due to the improper orientation and suboptimal distance between the ligands. The atoms directly involved in the formation of the covalent ternary intermediate and subsequent methyl transfer move apart by $\sim$1.20 Å. This fits well with the kinetic data showing slow formation of the covalent ternary intermediate in S290G as compared to that of the wild type. In addition, the kinetic data on the conformational change associated with CH_2H_4folate binding point to a role in formation of the iminium intermediate, the ring-opening step. Indeed, the formation of the covalent ternary intermediate has been shown to require the proper orientation of dUMP and CH_2H_4folate (*13*, *29*, *39*). Additionally, previous studies have shown that mutation of other active site residues implicated in imidazolidine ring opening (*40*, *41*) results in a drastic decrease in the rate of catalysis (*29*, *42*) and improperly aligned substrates (*39*). Altogether, this sheds light on Ala287 and Ser290 predominantly having a role in productive substrate positioning as opposed to simply providing an added interaction to stabilize ligand binding.

Our kinetic data and crystal structure presented here provide the first evidence explaining the unusually fast TS rate in *C. hominis*. When a key nonconserved residue is mutated to its conserved counterpart, the effect is an increase in distance between the substrates, resulting in a large decrease in the extent of ternary complex formation and subsequent catalytic rate. The decreased catalytic rate and binding affinity of CH_2H_4folate are on the order of those of the slower species of TS enzymes (*30*, *43*, *44*). Interestingly, the distance between the ligands in our *Ch*TS-DHFR mutant with a decreased rate approaches the positioning in these slower enzymes. Together with the data for the decreased rate of conformational changes leading to intermediate formation, it seems very likely that the unusually close positioning of substrates in *Ch*TS-DHFR is primarily responsible for the unusually fast TS rate.

Due to difficulty in initiating and maintaining a cellular model of *C. hominis*, physiological data elucidating the importance of a fast TS enzyme are lacking (*45*). However, completion of the *C. hominis* genome has established that the parasite relies solely on pyrimidine scavenging from the host for nucleotide biosynthesis (*46*, *47*). Additionally, *T. gondii*, another apicomplexan parasite, has displayed differential expression of two isoforms of a glycolytic enzyme. The parasite preferentially expresses the isoform with an increased catalytic rate during virulent reproductive stages, suggesting the need for more efficient nutrient utilization during growth (*48*). We propose that nonconserved residues Ser290 and Ala287 effect a high rate of TS catalysis that enables *C. hominis* to efficiently utilize the host pyrimidine nucleotides, affording the parasite a competitive advantage.

The fact that A287F and A287F/S290G mutant enzymes seem to have partially restored activity leads us to assume that the substrate movement in the context of Phe287 is not as drastic. Since residue 287 also contacts the folate glutamate tail, a phenylalanine at that position may restrict how far the folate can move away, therefore attenuating the subsequent movement of dUMP and the distance between the two. However, factors other than static substrate distance, such as ligand and enzyme flexibility, may play additional roles. Further structural studies on the mutant enzymes are underway to complement the kinetic data presented here.

ACKNOWLEDGMENT

We thank Dr. Amy C. Anderson for helpful discussions and Dr. Rick G. Nelson for the gift of plasmid. We also thank Michael Becker, Anand Saxena, Sal Sclafani, Stu Myers, and the entire staff at beamline X25 of the National Synchrotron Light Source at Brookhaven National Laboratory (Upton, NY) for their gracious technical help.

SUPPORTING INFORMATION AVAILABLE

HPLC elution profiles for TS single-turnover reactions for the identification of the intermediate as well as reaction time courses used in determining the rate of formation for dTMP and representative stopped-flow data for DHFR pre-steady-state burst and rapid chemical quench data for consumption of CH_2H_4folate. This material is available free of charge via the Internet at http://pubs.acs.org.

REFERENCES

1. Carreras, C. W., and Santi, D. V. (1995) The catalytic mechanism and structure of thymidylate synthase, *Annu. Rev. Biochem. 64*, 721−762.

2. Benkovic, S. J., and Hammes-Schiffer, S. (2003) A perspective on enzyme catalysis, *Science 301*, 1196−1202.
3. Stroud, R. M., and Finer-Moore, J. S. (2003) Conformational dynamics along an enzymatic reaction pathway: Thymidylate synthase, "the movie", *Biochemistry 42*, 239−247.
4. Santi, D. V., McHenry, C. S., Raines, R. T., and Ivanetich, K. M. (1987) Kinetics and thermodynamics of the interaction of 5-fluoro-2′-deoxyuridylate with thymidylate synthase, *Biochemistry 26*, 8606−8613.
5. Cox, K., Robertson, D., and Fites, R. (1999) Mapping and expression of a bifunctional thymidylate synthase, dihydrofolate reductase gene from maize, *Plant Mol. Biol. 41*, 733−739.
6. Anderson, K. S. (1999) Fundamental mechanisms of substrate channeling, *Methods Enzymol. 308*, 111−145.
7. Liang, P. H., and Anderson, K. S. (1998) Substrate channeling and domain-domain interactions in bifunctional thymidylate synthase-dihydrofolate reductase, *Biochemistry 37*, 12195−12205.
8. Atreya, C. E., and Anderson, K. S. (2004) Kinetic Characterization of Bifunctional Thymidylate Synthase-Dihydrofolate Reductase (TS-DHFR) from *Cryptosporidium hominis*: A Paradigm Shift for TS Activity and Channeling Behavior, *J. Biol. Chem. 279*, 18314−18322.
9. Stout, T. J., Schellenberger, U., Santi, D. V., and Stroud, R. M. (1998) Crystal structures of a unique thermal-stable thymidylate synthase from *Bacillus subtilis*, *Biochemistry 37*, 14736−14747.
10. Anderson, A. C., O'Neil, R. H., Surti, T. S., and Stroud, R. M. (2001) Approaches to solving the rigid receptor problem by identifying a minimal set of flexible residues during ligand docking, *Chem. Biol. 8*, 445−457.
11. Anderson, A. C., Perry, K. M., Freymann, D. M., and Stroud, R. M. (2000) The crystal structure of thymidylate synthase from *Pneumocystis carinii* reveals a fungal insert important for drug design, *J. Mol. Biol. 297*, 645−657.
12. O'Neil, R. H., Lilien, R. H., Donald, B. R., Stroud, R. M., and Anderson, A. C. (2003) Phylogenic classification of protozoa based on the structure of the linker domain in the bifunctional enzyme, dihydrofolate reductase-thymidylate synthase, *J. Biol. Chem. 278*, 52980−52987.
13. Huang, W., and Santi, D. V. (1994) Isolation of a covalent steady-state intermediate in glutamate 60 mutants of thymidylate synthase, *J. Biol. Chem. 269*, 31327−31329.
14. Kamb, A., Finer-Moore, J. S., and Stroud, R. M. (1992) Cofactor triggers the conformational change in thymidylate synthase: Implications for an ordered binding mechanism, *Biochemistry 31*, 12876−12884.
15. Dillingham, R., Lima, A., and Guerrant, R. (2002) Cryptosporidiosis: Epidemiology and impact, *Microbes Infect. 4*, 1059−1066.
16. Mathews, C. K., and Huennekens, F. M. (1960) Enzymic preparation of the L,L-diastereoisomer of tetrahydrofolic acid, *J. Biol. Chem. 235*, 3304−3308.
17. Curthoys, N. P., Scott, J. M., and Rabinowitz, J. C. (1972) Folate coenzymes of *Clostridium acidi-urici*. The isolation of L-5,10-methenyltetrahydropteroyltriglutamate, its conversion to L-tetrahydropteroyltriglutamate and L-10-[^{14}C]formyltetrahydropteroyltriglutamate, and the synthesis of L-10-formyl-(6,7-$^{3}H_2$)tetrahydropteroyltriglutamate and L-(6,7-$^{3}H_2$)tetrahydropteroyltriglutamate, *J. Biol. Chem. 247*, 1959−1964.
18. Kallen, R. G., and Jencks, W. P. (1966) The dissociation constants of tetrahydrofolic acid, *J. Biol. Chem. 241*, 5845−5850.
19. Johnson, E. F., Hinz, W., Atreya, C. E., Maley, F., and Anderson, K. S. (2002) Mechanistic characterization of *Toxoplasma gondii* thymidylate synthase (TS-DHFR)-dihydrofolate reductase. Evidence for a TS intermediate and TS half-sites reactivity, *J. Biol. Chem. 277*, 43126−43136.
20. Meek, T. D., Garvey, E. P., and Santi, D. V. (1985) Purification and characterization of the bifunctional thymidylate synthetase-dihydrofolate reductase from methotrexate-resistant *Leishmania tropica*, *Biochemistry 24*, 678−686.
21. Carreras, C. W., Climie, S. C., and Santi, D. V. (1992) Thymidylate synthase with a C-terminal deletion catalyzes partial reactions but is unable to catalyze thymidylate formation, *Biochemistry 31*, 6038−6044.
22. Otwinowski, Z., and Minor, W. (1997) Processing of X-Ray Diffraction Data Collected in Oscillation Mode, *Methods Enzymol. 276*, 307−326.
23. Collaborative Computational Project, Number 4 (1994) The CCP4 Suite: Programs for Protein Crystallography, *Acta Crystallogr. D50*, 760−763.
24. Murshudov, G. N., Vagin, A. A., and Dodson, E. J. (1997) Refinement of macromolecular structures by the maximum-likelihood method, *Acta Crystallogr. D53*, 240−255.
25. Jones, T. A., Zou, J. Y., Cowan, S. W., and Kjeldgaard, M. (1991) Improved methods for building protein models in electron density maps and the location of errors in these models, *Acta Crystallogr. A47* (Part 2), 110−119.
26. Emsley, P., and Cowtan, K. (2004) Coot: Model-Building Tools for Molecular Graphics, *Acta Crystallogr. D60*, 2126−2132.
27. Brunger, A. T., Adams, P. D., Clore, G. M., DeLano, W. L., Gros, P., Grosse-Kunstleve, R. W., Jiang, J. S., Kuszewski, J., Nilges, M., Pannu, N. S., Read, R. J., Rice, L. M., Simonson, T., and Warren, G. L. (1998) Crystallography & NMR system: A new software suite for macromolecular structure determination, *Acta Crystallogr. D54*, 905−921.
28. Anderson, A. C., O'Neil, R. H., DeLano, W. L., and Stroud, R. M. (1999) The structural mechanism for half-the-sites reactivity in an enzyme, thymidylate synthase, involves a relay of changes between subunits, *Biochemistry 38*, 13829−13836.
29. Sage, C. R., Rutenber, E. E., Stout, T. J., and Stroud, R. M. (1996) An essential role for water in an enzyme reaction mechanism: The crystal structure of the thymidylate synthase mutant E58Q, *Biochemistry 35*, 16270−16281.
30. Phan, J., Steadman, D. J., Koli, S., Ding, W. C., Minor, W., Dunlap, R. B., Berger, S. H., and Lebioda, L. (2001) Structure of human thymidylate synthase suggests advantages of chemotherapy with noncompetitive inhibitors, *J. Biol. Chem. 276*, 14170−14177.
31. Schiffer, C. A., Clifton, I. J., Davisson, V. J., Santi, D. V., and Stroud, R. M. (1995) Crystal structure of human thymidylate synthase: A structural mechanism for guiding substrates into the active site, *Biochemistry 34*, 16279−16287.
32. Schiffer, C. A., Davisson, V. J., Santi, D. V., and Stroud, R. M. (1991) Crystallization of human thymidylate synthase, *J. Mol. Biol. 219*, 161−163.
33. Cisneros, R. J., and Dunlap, R. B. (1990) Development of a trichloroacetic acid precipitation assay for covalent adducts of thymidylate synthase, *Anal. Biochem. 186*, 202−208.
34. Barshop, B. A., Wrenn, R. F., and Frieden, C. (1983) Analysis of numerical methods for computer simulation of kinetic processes: Development of KINSIM−a flexible, portable system, *Anal. Biochem. 130*, 134−145.
35. Pogolotti, A. L., Jr., Danenberg, P. V., and Santi, D. V. (1986) Kinetics and mechanism of interaction of 10-propargyl-5,8-dideazafolate with thymidylate synthase, *J. Med. Chem. 29*, 478−482.
36. Finer-Moore, J. S., Montfort, W. R., and Stroud, R. M. (1990) Pairwise specificity and sequential binding in enzyme catalysis: Thymidylate synthase, *Biochemistry 29*, 6977−6986.
37. Vasquez, J. R., Gooze, L., Kim, K., Gut, J., Petersen, C., and Nelson, R. G. (1996) Potential antifolate resistance determinants and genotypic variation in the bifunctional dihydrofolate reductase-thymidylate synthase gene from human and bovine isolates of *Cryptosporidium parvum*, *Mol. Biochem. Parasitol. 79*, 153−165.
38. Spencer, H. T., Villafranca, J. E., and Appleman, J. R. (1997) Kinetic scheme for thymidylate synthase from *Escherichia coli*: Determination from measurements of ligand binding, primary and secondary isotope effects, and pre-steady-state catalysis, *Biochemistry 36*, 4212−4222.
39. Birdsall, D. L., Huang, W., Santi, D. V., Stroud, R. M., and Finer-Moore, J. (1998) The separate effects of E60Q in *Lactobacillus casei* thymidylate synthase delineate between mechanisms for formation of intermediates in catalysis, *Protein Eng. 11*, 171−183.
40. Hardy, L. W., Graves, K. L., and Nalivaika, E. (1995) Electrostatic guidance of catalysis by a conserved glutamic acid in *Escherichia coli* dTMP synthase and bacteriophage T4 dCMP hydroxymethylase, *Biochemistry 34*, 8422−8432.
41. Sage, C. R., Michelitsch, M. D., Stout, T. J., Biermann, D., Nissen, R., Finer-Moore, J., and Stroud, R. M. (1998) D221 in thymidylate synthase controls conformation change, and thereby opening of the imidazolidine, *Biochemistry 37*, 13893−13901.
42. Cisneros, R. J., Zapf, J. W., and Dunlap, R. B. (1993) Studies of 5-fluorodeoxyuridine 5′-monophosphate binding to carboxypeptidase A-inactivated thymidylate synthase from *Lactobacillus casei*, *J. Biol. Chem. 268*, 10102−10108.
43. Fantz, C., Shaw, D., Jennings, W., Forsthoefel, A., Kitchens, M., Phan, J., Minor, W., Lebioda, L., Berger, F. G., and Spencer, H. T. (2000) Drug-resistant variants of *Escherichia coli* thymidylate

synthase: Effects of substitutions at Pro-254, *Mol. Pharmacol. 57*, 359−366.
44. Steadman, D. J., Spencer, H. T., Dunlap, R. B., and Berger, S. H. (1999) Substitution at residue 214 of human thymidylate synthase alters nucleotide binding and isomerization of ligand-protein complexes, *Biochemistry 38*, 5582−5587.
45. Tzipori, S., and Ward, H. (2002) Cryptosporidiosis: Biology, pathogenesis and disease, *Microbes Infect. 4*, 1047−1058.
46. Striepen, B., Pruijssers, A. J., Huang, J., Li, C., Gubbels, M. J., Umejiego, N. N., Hedstrom, L., and Kissinger, J. C. (2004) Gene transfer in the evolution of parasite nucleotide biosynthesis, *Proc. Natl. Acad. Sci. U.S.A. 101*, 3154−3159.
47. Xu, P., Widmer, G., Wang, Y., Ozaki, L. S., Alves, J. M., Serrano, M. G., Puiu, D., Manque, P., Akiyoshi, D., Mackey, A. J., Pearson, W. R., Dear, P. H., Bankier, A. T., Peterson, D. L., Abrahamsen, M. S., Kapur, V., Tzipori, S., and Buck, G. A. (2004) The genome of *Cryptosporidium hominis*, *Nature 431*, 1107−1112.
48. Dzierszinski, F., Mortuaire, M., Dendouga, N., Popescu, O., and Tomavo, S. (2001) Differential expression of two plant-like enolases with distinct enzymatic and antigenic properties during stage conversion of the protozoan parasite *Toxoplasma gondii*, *J. Mol. Biol. 309*, 1017−1027.

BI700531R